Some Stuttgart Highlights of Photogrammetry and Remote Sensing

Dieter Fritsch, Stuttgart

ABSTRACT

The Institute for Photogrammetry at the University of Stuttgart has made substantial contributions to photogrammetry since its launch on April 1st, 1964, first under the supervision of Fritz Ackermann. Since June 1st, 1992 Dieter Fritsch suceeded and continued the profile in photogrammetry, but started R&D in remote sensing and geoinformatics as well. In the following some highlights of the last decade are given to demonstrate the performance of an university institute to investigate open issues in research, developments and applications. Following some proposals of the 1970s and 1980s new concepts for camera self-calibration are given, and the dense image matching software SURE is successfully succeeding the area-and feature-based matching algorithms. Most recently a comprehensive study was started to exploit the potential of SURE for DSM generation of High Resolution satellite imagery, such as WorldView-2.

1. INTRODUCTION

Early work right after the launch of the Institute for Photogrammetry started with R&D in aerial triangulation. The famous software packages PAT-M and PAT-B became a standard of many mapping associations worldwide (Ackermann, 1981). Camera calibration seemed to be and still is an essential subject not only in photogrammetry, but also in computer vision and optical engineering. Self-calibration by using additional parameters (APs) has been widely accepted and substantially utilized as an efficient calibration technique in the photogrammetric society since the 1970s. It plays a significant role in the automatic interior/exterior orientation of camera systems. Many studies investigated the use of self-calibration APs in the last decades. Traditionally, two types of self-calibration APs were developed for *analogue* single-head camera calibration: physical and mathematical. The development of physical APs was mainly attributed to Brown (1971) for close-range camera calibration and these APs were later extended for aerial applications (Brown, 1976). El-Hakim & Faig (1977) proposed mathematical APs by using spherical harmonics. Ebner (1976) and Grün (1978) built the second and the fourth order algebraic polynomial APs, respectively. These early works showed the remarkable significance of self-calibration APs in reducing the image residuals and improving the external accuracy of aerial triangulation, while all the time concerns have been raised on over-parameterization and high correlations (Kilpelä, 1981; Clarke & Fryer, 1998). The quite popular polynomial APs are often criticized as “they have no foundations based on observable physical phenomena” (Clarke & Fryer, 1998; McGlone et al., 2004).

These APs, though being widely used for many years and even in the digital era, might be however inadequate to fit the distinctive features of *digital* airborne cameras, such as push-broom, multi-head, virtual images composition, various image formats (Honkavaara et al., 2006; Cramer, 2009). A considerable progress was made for digital camera calibration. The self-calibration APs were investigated in Fraser (1997) for digital close-range camera calibration. Cramer (2009) and Jacobsen et al. (2010) reported the comprehensive empirical tests, in which lots of different APs were employed to compensate the image distortion. But the inconveniences still remained. Firstly, many APs are purely the combinations of the traditional APs and they might be inadequate. Secondly, some APs are designed and used without evident physical or mathematical foundations (Clarke & Fryer, 1998). Thirdly, some APs suffer for high correlations with interior orientation (IO) parameters or other correction parameters (Cramer, 2009). Last but not least, some are tailored for the specific cameras concerning the manufacturing technology. They can hardly be used to calibrate different cameras in

a general sense. The topic of using additional parameters for camera self-calibration was – in our opinion – not yet solved satisfactorily in 2010, when ifp started to re-launch R&D work for this issue (see chapter 2).

Image matching is an issue of extensive R&D of ifp since the early 1980s, when first investigations were made for area-based least squares correlations (Ackermann, 1983). Soon after, feature-based image matching was exploited and served for many years for the automation of aerial triangulation (Foerstner, 1986, Tsingas, 1992). With the invention of Semi-Global Matching (SGM) by Hirschmueller (2005) the paradigm of image matching changed completely. The pixel-wise image matching provides very dense point clouds of superior quality. Nowadays, most vendors of photogrammetric hardware, software and workflows offer a DIM (Dense Image Matching) software module.

The development of the software SURE – SUrface REconstruction Using Imagery started at the Institute for Photogrammetry (ifp) early 2010 with consulting work for MS Vexcel (an OpenPhoWo Partner since 2003), Graz, when the potential of dense image matching algorithms had to be proven for UltraCam's aerial imagery. Soon after, another feasibility study was performed for VisionMap (another OpenPhoWo Partner since 2013), Tel Aviv, processing its A3 image blocks (Fritsch & Rothermel, 2013) for the generation of 3D building models. A close cooperation for more than two decades between IGI, Kreuztal (also an Open PhoWo Partner since 2003) and the ifp gave reason to exploit also the potential of DigiCam imagery for dense imaging matching. The follow-up of this cooperation is given in Grimm (2015). Moreover, in 2011 the ifp took over responsibilities to reconstruct the Tympana of the Royal Palace Amsterdam, The Netherlands, with methods of close range photogrammetry employing Structure-from-Motion and DIM algorithms (Fritsch et al., 2011). Needless to say that SURE was demanded by National Mapping Agencies already in its infancy stage of implementation and proven to generate high density point clouds. Since 2013 further developments of SURE are outsourced into the Startup nFrames GmbH, Stuttgart, which is offering SURE in a professional environment. An update of SURE is given in chapter 3.

Chapter 4 reflects a feasibility study using high resolution satellite imagery, such as WorldView-2, to be prepared to process the 0.31cm GSD of WordView-3 images in future. Here it is interesting to reconstruct the geometry of the satellite orbits by means of a photogrammetric bundle block adjustment, especially when overlapping stereo scenes can be created. The Rational Polynomial Coefficients are transformed to a classical photogrammetric image model using an affine transformation in image space, to perform the estimation of exterior orientation parameters. With this information the SURE processing pipeline can be started, with some modifications with regard to the disparity estimation. For this study the Munich WV-2 stereo scenes have been chosen, because there is good reference data available: The LiDAR DEM and the aerial photo DSM processed for the EuroSDR Benchmark for Dense Image Matching. After the image orientations the WV-2 DSM is created and compared with the reference delivering RMS in height of about 1,4m over roof surfaces and 2m on the ground.

The paper is concluded with a summary of the findings in camera calibration and some experiences using dense image matching in many projects.

2. CAMERA CALIBRATION – THE NEW APPROACH

All the above introductory statements motivated us to investigate the problem of airborne camera self-calibration from scratch. For the PhD work of Tang (2013) one main strategy was followed all

the time: Photogrammetric self-calibration can be considered – to a very large extent – as a *function approximation* problem in mathematics. An intrinsic deficiency of polynomial APs is revealed. Algebraic polynomials are not proper for self-calibration purpose from a mathematical point of view. By examining different mathematical bases, Fourier series (trigonometric polynomials) are favored as the optimal mathematical basis functions for building self-calibration APs. Then, a whole family of so-called *Fourier self-calibration APs* is developed. Fourier APs are orthogonal, mathematically rigorous, flexible, generic and efficient for calibrating the image distortion of all frame airborne cameras. The advantages of Fourier APs have been demonstrated over the polynomial APs and the physical APs. Their performance is evaluated in several empirical tests.

2.1. Fourier Self-Calibration Parameters

The collinearity equation, which is the mathematical fundamental of photogrammetry, is given in (1).

$$\begin{aligned} x &= x_0 - c\frac{r_{11}(X-X_0)+r_{21}(Y-Y_0)+r_{31}(Z-Z_0)}{r_{13}(X-X_0)+r_{23}(Y-Y_0)+r_{33}(Z-Z_0)} + \Delta x + \varepsilon \\ y &= y_0 - c\frac{r_{12}(X-X_0)+r_{22}(Y-Y_0)+r_{32}(Z-Z_0)}{r_{13}(X-X_0)+r_{23}(Y-Y_0)+r_{33}(Z-Z_0)} + \Delta y + \varepsilon \end{aligned} \tag{1}$$

where Δx and Δy denote image distortion, ε random error. The other notations can be seen in textbooks such like Kraus (2007). The distortion terms are functions of two variables and their functional forms are unknown. They need to be approximated by parametric models, i.e., self-calibration APs.

Based on the standard 60% forward overlapping level and the 3×3 and 5×5 grid pattern of image point distribution, Ebner (1976) and Grün (1978) proposed the second and the fourth order polynomial APs, respectively. Although they constructed their polynomial APs without using explicitly the function approximation principle, we showed that, both sets of APs can be exactly derived from this principle (Tang et al., 2012a). The mathematical theorem behind them is the well-defined Weierstrass Theorem, which indicates that any function can be approximated with arbitrary accuracy by a polynomial of sufficiently high degree (Oliver et al., 2010). Both sets of APs can compensate the image distortion, because polynomials can approximate any unknown distortion function, according to the Weierstrass Theorem. From the approximation principle, it can be easily explained that the regular grid pattern is not a prerequisite for applying both APs. The main effect of the irregular image point distribution is degrading correlations but not decaying calibration. This is the exact reason why Ebner and Grün models still work quite well in cases where the ideal regular grid pattern is unsatisfied.

In fact, we have developed in our previous work a new family of so-called *Legendre self-calibration APs*, which is established on the basis of the orthogonal univariate Legendre Polynomials. The mathematical relations can be derived between Legendre APs and the two historical APs. From both theoretical analyses and practical test results, Legendre APs can also be considered as the superior generalization of the Ebner and Grün models in many senses. The Legendre APs of second and fourth order must be preferred to the Ebner and Grün models, respectively (Tang et al., 2012a).

However, there is an intrinsic deficiency of all polynomial APs, including Ebner, Grün and Legendre APs. That is, all polynomial APs need to eliminate four highly correlated parameters (another two of six, i.e. two constant terms, are eliminated because they are merely principle point shifts. The removal

of these two constant terms is NOT caused by high correlation). The elimination imposes four constraints on polynomial APs. For example, the constraints on Legendre APs are shown in (2),

$$\begin{aligned}(\Delta x): &\quad +a_1 p_{1,0} + a_2 p_{0,1} + a_3 p_{2,0} + a_4 p_{1,1} \\ (\Delta y): &\quad +a_2 p_{1,0} - a_1 p_{0,1} - a_3 p_{1,1} - a_4 p_{0,2}\end{aligned} \tag{2}$$

This occurs exactly to the Ebner and Grün models as well. These four constraints, which are caused by high correlations, violate the mathematical principle of polynomial APs. According to the approximation theory and the Weierstrass Theorem, all APs in Δx should be fully independent of those in Δy. In other words, the theoretical number of unknowns in Ebner, Grün and the fifth order Legendre APs should be 16, 48 and 70, rather than 12, 44 and 66, respectively. The elimination, which is indispensable for constructing polynomial APs, degrades the rigorousness of polynomial APs. It may produce negative effects in calibration.

Besides the algebraic polynomials, other basis functions are an alternative for developing mathematical APs. Here the mathematical basis functions for the function approximation applications are briefly reviewed. Three groups of quite useful basis functions can be derived from the renowned Laplace Equation, depending on the defined coordinate systems. The Laplace Equation in two variables is given in (3).

$$\frac{d^2 f}{dx^2} + \frac{d^2 f}{dy^2} = 0 \tag{3}$$

The three basis functions derived from (3) are: Fourier series (trigonometric polynomials) for the Cartesian coordinates, Bessel functions for the cylindrical coordinates and spherical harmonics (or circular harmonics in two-dimension) for the spherical coordinates. Wavelet functions and rational functions are also useful for specific implementations. For more on the function approximation theory, the readers are referred to textbooks such as Oliver et al. (2010).

For the self-calibration purpose, wavelet functions are not appropriate mainly since of its non-analytical form, which precludes them from being incorporated into (1). The form of rational functions is rather inconvenient and can burden the adjustment. For the three functions from Laplace Equation, Fourier series should be favored, as their Cartesian coordinates are defined in the rectangular image format. This mathematical insight also explains why the APs using spherical harmonics (El-Hakim & Faig, 1977) are less significant in practice. Actually, the APs using spherical harmonics encounter similar difficulties of high correlation as the algebraic polynomial APs. Therefore, we develop below the self-calibration APs on the basis of Fourier series.
Bivariate Fourier series are given in (4).

$$\cos(mx \pm ny), \sin(mx \pm ny), \quad m, n = 0, 1, 2, \ldots \tag{4}$$

where $x, y \in [-\pi, \pi]$. The Fourier Theorem indicates that any two-variable functions, defined in $[-\pi, \pi] \times [-\pi, \pi]$, can be approximated with arbitrary accuracy by the combination of the bivariate Fourier series of sufficiently high degree.
Let $2b_x$ and $2b_y$ denote the width and length of the image format, respectively. x and y indicate the metric coordinate of the image measurement, $-b_x \le x \le b_x, -b_y \le y \le b_y$. Denote

$$
\begin{aligned}
&u = x\pi / b_x, \quad v = y\pi / b_y, \qquad u, v \in [-\pi, \pi] \\
&c_{m,n} = \cos(mu + nv), \quad s_{m,n} = \sin(mu + nv)
\end{aligned} \tag{5}
$$

The $c_{m,n}$ and $s_{m,n}$ satisfy the orthogonal equations (6), which indicates $c_{m,n}$ and $s_{m,n}$ are orthogonal over the whole image dimension.

$$
\begin{aligned}
&\int_{-b_y}^{b_y}\int_{-b_x}^{b_x} c_{m,n}c_{m',n'}dxdy = 0, \quad if\ m \neq m'\ or\ n \neq n' \\
&\int_{-b_y}^{b_y}\int_{-b_x}^{b_x} s_{m,n}s_{m',n'}dxdy = 0, \quad if\ m \neq m'\ or\ n \neq n' \\
&\int_{-b_y}^{b_y}\int_{-b_x}^{b_x} c_{m,n}s_{m',n'}dxdy = 0
\end{aligned} \tag{6}
$$

Then, we use the linear combination of the bivariate Fourier series to approximate the distortion terms Δx and Δy, respectively. From (4)-(6), the general form of self-calibration models is obtained in (7).

$$
\begin{aligned}
\Delta x &= \sum_{m=1}^{M}\sum_{n=-N}^{n=N}\left(a_{m,n}c_{m,n} + b_{m,n}s_{m,n}\right) + \sum_{n=1}^{N}\left(a_{0,n}c_{0,n} + b_{0,n}s_{0,n}\right) \\
\Delta y &= \sum_{m=1}^{M}\sum_{n=-N}^{n=N}\left(a'_{m,n}c_{m,n} + b'_{m,n}s_{m,n}\right) + \sum_{n=1}^{N}\left(a'_{0,n}c_{0,n} + b'_{0,n}s_{0,n}\right)
\end{aligned} \tag{7}
$$

where $a_{m,n}$, $b_{m,n}$, $a'_{m,n}$ and $b'_{m,n}$ are the unknown coefficients (parameters) to be computed in a bundle block adjustment. M and N are the maximum degrees chosen by the users (generally speaking, the more complicated the distortion is, the larger M and N are required). The number of unknown APs is $2(2M(2N+1)+2N) = 4(2MN + M + N)$.

This family of self-calibration APs (with respect to the chosen M and N) is based on Fourier series, thus they are named as *Fourier self-calibration APs*. Note that in (7) the unknown parameters in Δx are fully independent of those in Δy. (Interestingly, a few terms of the Fourier series were employed in Jacobsen (2007). However, it must be noticed those terms were entirely different from the Fourier APs in our work).
Particularly, the Fourier APs of $M = N = 1$ (16 unknowns) are given with lexicographic order in (8).

$$
\begin{aligned}
\Delta x &= a_1c_{1,0} + a_2c_{0,1} + a_3c_{1,-1} + a_4c_{1,1} + a_5s_{1,0} + a_6s_{0,1} + a_7s_{1,-1} + a_8s_{1,1} \\
\Delta y &= a_9c_{1,0} + a_{10}c_{0,1} + a_{11}c_{1,-1} + a_{12}c_{1,1} + a_{13}s_{1,0} + a_{14}s_{0,1} + a_{15}s_{1,-1} + a_{16}s_{1,1}
\end{aligned} \tag{8}
$$

The Fourier APs of $M = N = 2$ with 48 unknowns are in (9).

$$
\begin{aligned}
\Delta x &= a_1c_{1,0} + a_2c_{0,1} + a_3c_{2,0} + a_4c_{1,-1} + a_5c_{1,1} + a_6c_{0,2} + a_7c_{1,2} + a_8c_{1,-2} \\
&+ a_9c_{2,-1} + a_{10}c_{2,1} + a_{11}c_{2,-2} + a_{12}c_{2,2} + a_{13}s_{1,0} + a_{14}s_{0,1} + a_{15}s_{2,0} + a_{16}s_{1,-1} \\
&+ a_{17}s_{1,1} + a_{18}s_{0,2} + a_{19}s_{1,2} + a_{20}s_{1,-2} + a_{21}s_{2,-1} + a_{22}s_{2,1} + a_{23}s_{2,-2} + a_{24}s_{2,2} \\
\Delta y &= a_{25}c_{1,0} + a_{26}c_{0,1} + a_{27}c_{2,0} + a_{28}c_{1,-1} + a_{29}c_{1,1} + a_{30}c_{0,2} + a_{31}c_{1,2} + a_{32}c_{1,-2} \\
&+ a_{33}c_{2,-1} + a_{34}c_{2,1} + a_{35}c_{2,-2} + a_{360}c_{2,2} + a_{37}s_{1,0} + a_{38}s_{0,1} + a_{39}s_{2,0} + a_{40}s_{1,-1} \\
&+ a_{41}s_{1,1} + a_{42}s_{0,2} + a_{43}s_{1,2} + a_{44}s_{1,-2} + a_{45}s_{2,-1} + a_{46}s_{2,1} + a_{47}s_{2,-2} + a_{48}s_{2,2}
\end{aligned} \tag{9}
$$

An intermediate between the first and the second order Fourier APs is given in (10), with 32 unknowns.

$$\begin{aligned}\Delta x &= a_1c_{1,0} + a_2c_{0,1} + a_3c_{2,0} + a_4c_{1,-1} + a_5c_{1,1} + a_6c_{0,2} + a_7c_{1,2} + a_8c_{1,-2} \\ &+ a_9c_{2,-1} + a_{10}c_{2,1} + a_{11}c_{2,-2} + a_{12}c_{2,2} + a_{13}s_{1,0} + a_{14}s_{0,1} + a_{15}s_{1,-1} + a_{16}s_{1,1} \\ \Delta y &= a_{17}c_{1,0} + a_{18}c_{0,1} + a_{19}c_{2,0} + a_{20}c_{1,-1} + a_{21}c_{1,1} + a_{22}c_{0,2} + a_{23}c_{1,2} + a_{24}c_{1,-2} \\ &+ a_{25}c_{2,-1} + a_{26}c_{2,1} + a_{27}c_{2,-2} + a_{28}c_{2,2} + a_{29}s_{1,0} + a_{30}s_{0,1} + a_{31}s_{1,-1} + a_{32}s_{1,1}\end{aligned} \tag{10}$$

2.2 Practical Tests

The Fourier self-calibration APs are comprehensively tested by using the data from the recent DGPF (German Society for Photogrammetry, Remote Sensing and Geoinformation) project, which was performed under the umbrella of DGPF and carried out in the test field Vaihingen/Enz nearby Stuttgart, Germany. This successful project aimed at an independent and comprehensive evaluation on the performance of digital airborne cameras, as well as offering a standard empirical dataset for the next years. The readers are referred to Cramer (2010) for more details.

Four datasets of the frame cameras are adopted: DMC (GSD 20cm, ground sample distance), DMC (GSD 8cm), UltracamX (GSD 20cm) and UltracamX (GSD 8cm). Each camera was flown at two heights. For each flight, we are interested in two most often scenarios: the in-situ calibration and the operational one. In the following the results of the operational scenario is given. There are 4 GCPs and 20% side-overlapping level in each block. The IMU misalignment, IO parameters and the Fourier APs with $M = N = 1$ are employed in the adjustment. This derived external accuracy is analogously denoted as "self calibrating" one. Due to 4 GCPs available only, the GPS/IMU observations have to be weighted carefully to achieve the best accuracy.

We also evaluated the quality of the in-situ calibration (Tang, 2012b). The calibration results of IO parameters and image distortion are utilized as fixed known values in the adjustment of the corresponding "reduced" operational block. It assumes the cameras have been fully calibrated. Self-calibration is not needed while the IMU misalignment correction parameters are still free unknown. The derived external accuracy is named as "after calibration". We compare "after calibration" with "self calibrating", "without APs" and theoretical accuracy.

The external accuracy results are illustrated in Fig. 1. On the one hand, the self-calibrating Fourier APs help to improve the external accuracy. It is noticed that for the blocks of weak geometry the accuracy in vertical direction is generally worse than 0.5 GSD. The "after calibration" yields more remarkable refinement in all four blocks, particularly in the vertical accuracy. The "after calibration" accuracy is very close to the optimal theoretical one in every block. Therefore, these tests not only recognize sufficient accuracy obtained by Fourier APs in the operational projects, but also confirm again their high efficiency in in-situ calibration. Besides, from the considerable distinction between "self-calibration" and "after calibration" accuracy in Fig. 1, it demonstrates the necessity of in-situ calibration in the presence of significant image distortion.

Additional tests on Fourier APs have been performed by using the data of other camera systems, including the medium-format DigiCAM, large-format UltracamXp and single-head DMC II cameras. The similarly good performance of Fourier APs is confirmed in these tests.

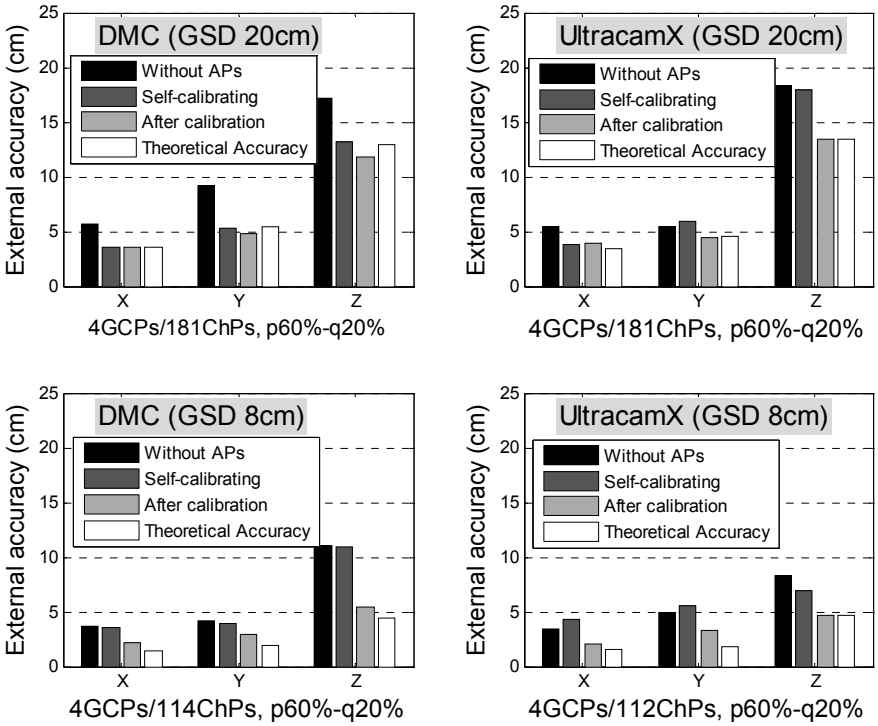

Figure 1: External accuracy in the four blocks of an operational project scenario, sparse GCPs and p60%-q20% ('without APs' indicates without using Fourier APs only).

More details and test results of this new approach for aerial camera calibration are given in Tang et al. (2012a, 2012b) and Tang (2013). Hopefully, aerial camera calibration in future is using this thorough and comprehensive modelling set of Fourier APs.

3. SURE – PHOTOGRAMMETRIC SURFACE RECONSTRUCTION FROM IMAGERY

The dense image matching solution SURE, as presented in Rothermel et al. (2012) and the previous Photogrammetric Week (Wenzel et al., 2013), is a scalable solution for the retrieval of dense 3D point clouds and digital surface models, with particular focus on large datasets and high precision requirements in professional surface productions.

3.1 Recent Developments – An Update

Since the previous Photogrammetric Week SURE has been enhanced by further options, such as the automatic generation of True Orthophotos (see Fig. 2), which are created by reprojecting the original imagery onto the DSM while refining edges and preserving the full 16 Bit radiometric information for four channels. In order to obtain full coverage also for occluded areas, several interpolation methods can be applied, which assure consistent results across spatially neighboring tiles. Scalable point cloud filtering in 2.5D and full 3D has been integrated, in order to enable the processing of oblique medium frame sensors and close range applications. Additional rectification methods have been added as well, in order to be able to process in-sequence datasets such as monocular corridor acquisition. This process is described in detail in the section 3.1.1.
Furthermore, a new approach of generating textured mesh surfaces for 2.5D and 3D workflows is explained with examples for several datasets.

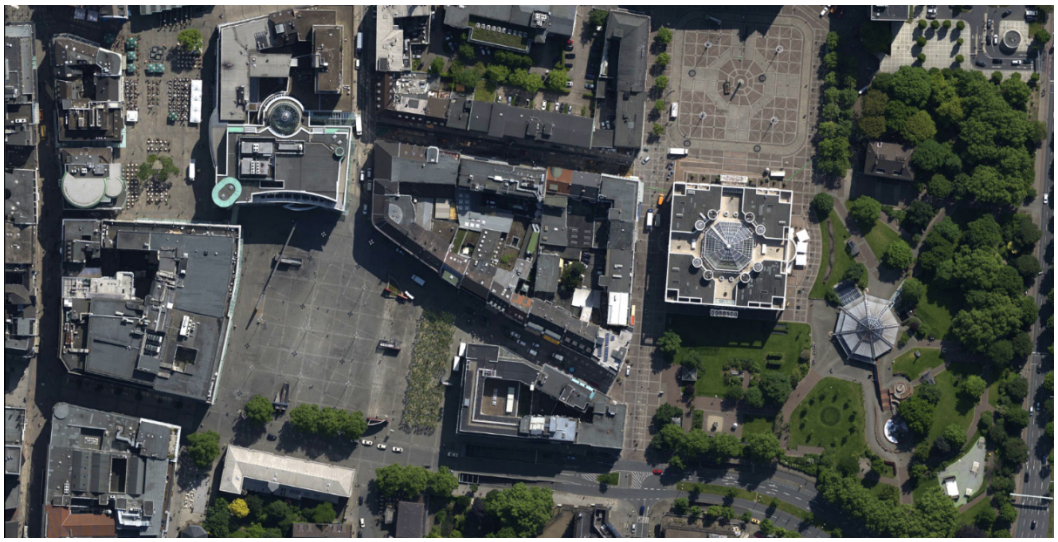

Figure 2: True Orthophoto with 10cm resolution retrieved automatically using SURE.

3.1.1 In-Sequence Dense Stereo

The work flow of depth map approaches for dense stereo is typically split into two processing steps: rectification of image pairs and subsequent generation of dense disparity maps. Various methodologies were proposed for image rectification, where images are re-sampled such that epipolar lines across an image pair are horizontal and object points are mapped to identical rows. However, homography-based methods as given by Fusiello et al., (2000) and Loop & Zhang (1999) lack the capability of rectifying image pairs which were acquired with motion in viewing direction – in particular for pure forward motion, where the epipoles in images are close or equal to zero. The rectified image pairs derived using the before mentioned rectification methods possess significant distortions and huge image dimensions. The pure-forward motion configuration merely occurs for traditional nadir airborne image blocks but is of greater relevance for data collected by image-based mobile mapping systems or UAV systems. The limitation for pure-forward motion pairs can be overcome by re-parametrization of Cartesian image coordinates to Polar image coordinates (with the origin located in the epipole) and the concept of half epipolar lines as proposed by Pollefeys et al. (1999). The approach was adapted and implemented into the SURE workflow including an automatic detection of an optimal stereo method. Fig. 3a shows an example of polar-rectified image pairs, and Fig. 3b depicts a point cloud produced from pure forward motion collected image pairs.

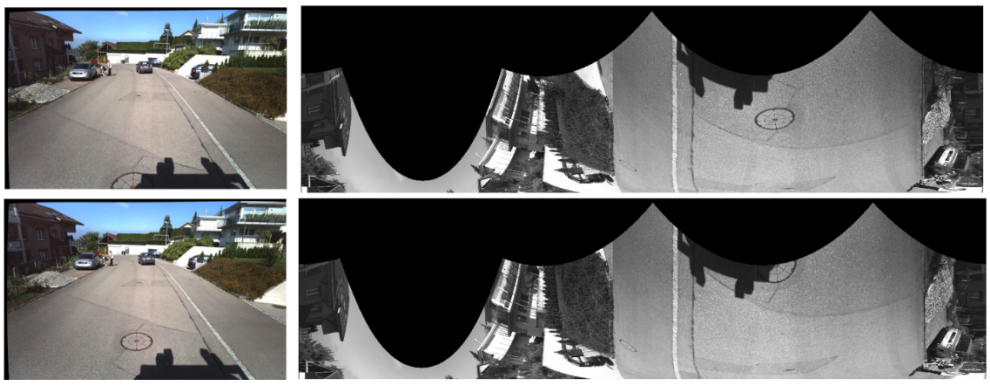

Figure 3a: Left: Original images from pure forward motion. Right: Polar rectified images, epipolar lines are vertical in this example.

Figure 3b: Point cloud generated by in sequence matching.

3.1.2 Generation of 2.5D Meshes

Typically in traditional nadir airborne flight missions, imagery is collected with limited viewing directions. As a result, the computed geometry of the scene can be represented sufficiently good by 2.5D digital surface models, also known as elevation maps. However, by utilizing camera systems possessing wide opening angles real 3D structure, as for example façades, are mapped, although with limited redundancy only. Latter and the fact that these surfaces most often are heavily slanted with respect to the viewing direction hinders reliable and dense reconstruction of these surface areas. However, the texture information can be used for texturing models for visualization. For this purpose we first have to extract a mesh representation from the DSMs. To reduce the number of triangles, we only consider elevation points contributing to the geometry and neglect data points in or close to the noise level. An ideal framework possessing this capability are restricted quadtrees as proposed in Payarola (1998). Beside a controlled way of data reduction the algorithm guarantees crack-free triangulations. An example of a triangulation is depicted in Fig. 4. Although these 2.5D meshes possess well shaped triangles for surfaces parallel to the DSM plane, badly shaped triangles are extracted at large elevation discontinuities, which implies non-robust normals. Since this is problematic for texture mapping, we re-mesh these areas by artificially sub-dividing, smoothing and fusing triangles.

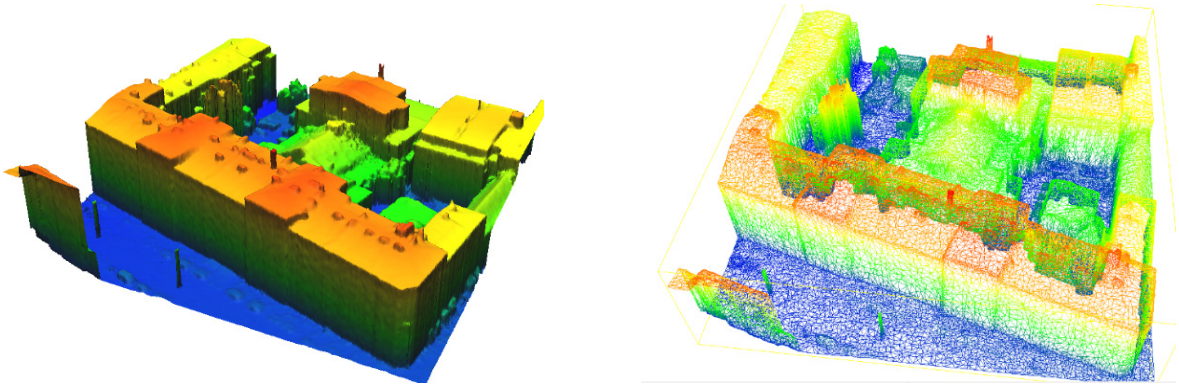

Figure 4: Color-coded visualization of 2.5D Surface Meshes generated from the Munich data set (Nadir Configuration, GSD 10 cm, Overlap: 80% in strip, 80% across strip).

These meshes then are textured following Waechter et al. (2014). An example is depicted in Fig. 5. Since we follow a processing scheme based on spatial tiles, the process scales well and enables mesh extraction of country wide projects. Even more impressive results can be obtained when utilizing oblique imagery.

Figure 5: Textured mesh automatically generated from the Munich EuroSDR data set (Haala, 2014) (Nadir Configuration, GSD 10 cm, Overlap: 80% in strip, 80% across strip).

3.1.3 Generation of 3D Meshes

The reconstruction algorithms in SURE can be characterized as depth map based, for details the interested reader is referred to Rothermel et al. (2012). Thereby for each base image a depth map is generated holding pixel-wise depth estimates, which are fused in order to obtain consistent surfaces. For the reconstruction of 2.5D surfaces this process can be tackled by gridding approaches, however when dealing with true 3D structure this task is not trivial. Beside a consistent surface representation, the fusion process aims at the reduction of outliers and improvement of precision of surface points,

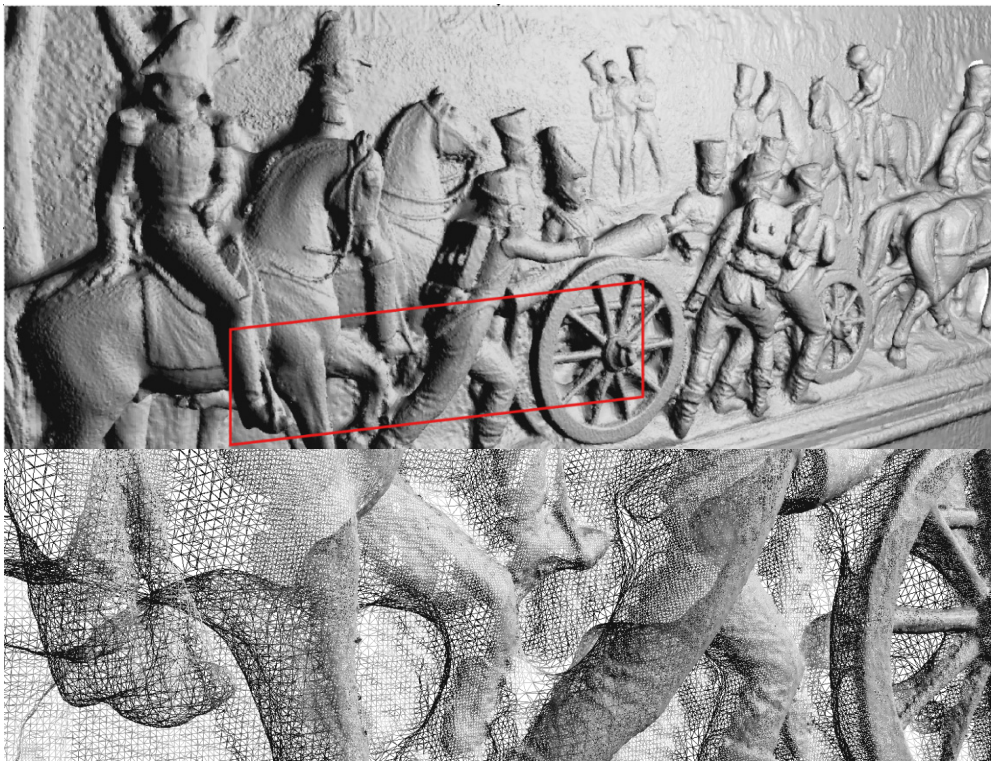

Figure 6: 3D Reconstruction of a Stuttgart Relief “The Battle of Brienne”.

while retrieving robust surface normals. The implementation of SURE follows a sequential approach. The current model state, represented as triangle mesh, is projected to the depth map which should be added. The depth map itself is subject to a RQT-based triangulation. Redundant triangles are identified and the best entity is selected based on robustness and precision. Sequentially processing of all depth maps leads to the final surface patches, or oriented points from which a water tight mesh can be reconstructed using for example Kashdan&Hoppe (2013). Texturing is carried out similar to the approach mentioned in section 2.5D meshes (see Fig. 6).

4. GEOMETRIC PROCESSING OF WORLDVIEW-2 IMAGERY

A feasibility study (Master's Thesis) was made to use WorldView-2 stereo scenes as input for creating a dense Digital Surface Model of Munich, Germany (Gong, 2015). The satellite stereo images are provided by the Deutsche Zentrum für Luft und Raumfahrt (DLR), Oberpfaffenhofen – in total there are four WorldView-2 images so that two pairs of stereo image could be processed. The imagery is generated on July 12, 2010, and delivered at Level 1B (the images are radiometrically and geometrically corrected but not projected onto a plane using any map projection). Each image spans approximate 20 x 15sqkm and comprises the main urban area of Munich at around 0.5 GSD. Fig. 7 shows an example of the stereo images.

The WorldView-2 dataset also provided the corresponding Rational Polynomial Coefficients (RPCs), but no GCPs. As most of the GCPs' coordinates in Germany are in the Gauss-Krueger coordinate system based on the Bessel ellipsoid they have to be transformed to the UTM coordinate system with the WGS84 reference ellipsoid.

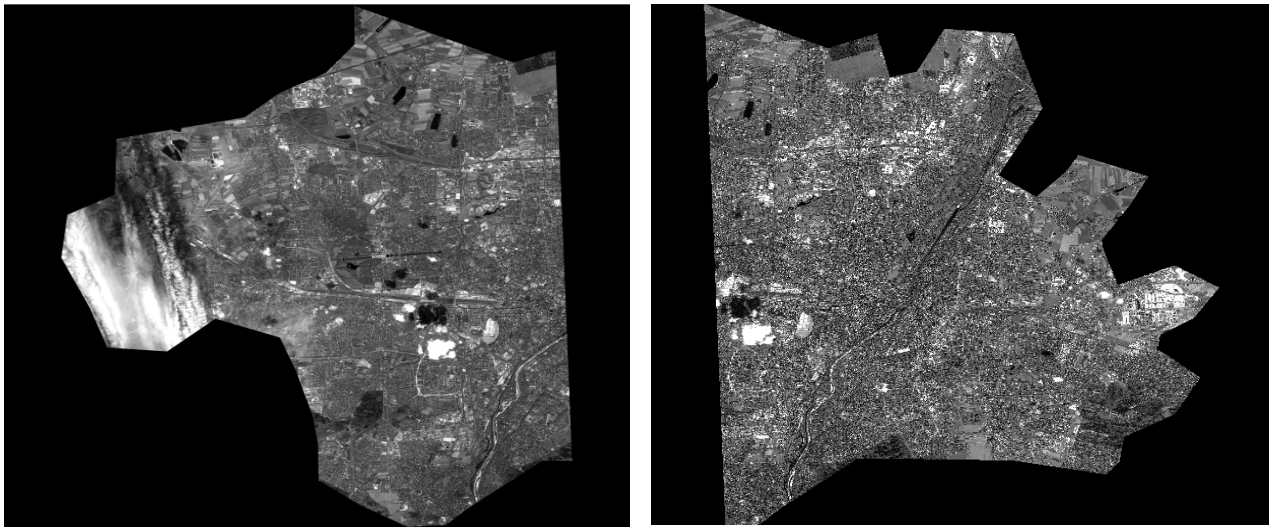

Figure 7: WorldView-2 stereo image of Munich. Copyright: DigitalGlobe

Besides GCP coordinates the National Mapping Agency of Bavaria (LDBV) provided an orthophoto with 20cm GSD and an aerial LiDAR point cloud. Processing the point cloud, a DEM with 50cm GSD became available (see Fig. 8a). The locations of ground control points are chosen by using the software ArcMap and then interpolated within the Digital Elevation Model (DEM). Ground control points are chosen from the points located on the ground, such as road intersections, tips of zebra lines or corners of playgrounds.

Figure 8: (a) Munich LiDAR DEM.

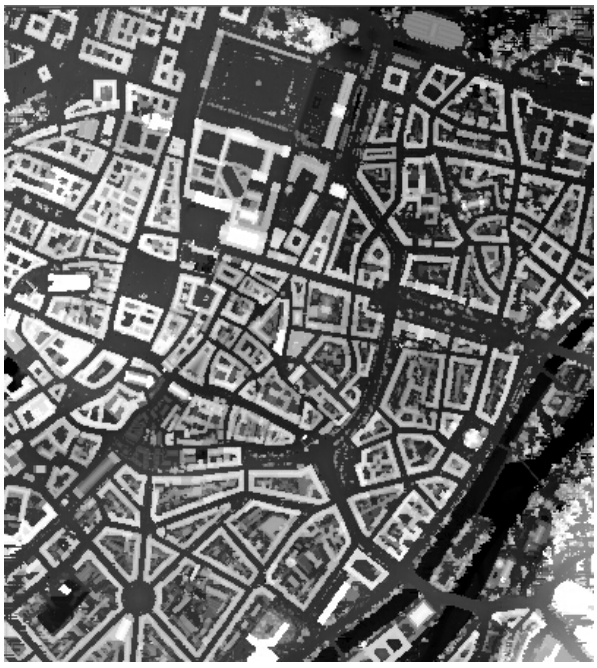

(b) Munich aerial photography DSM.

4.1. Satellite Image Orientation

Usually the satellite imagery providers deliver eighty RPCs along the images to users. A generalized model can be derived from RPCs, which can present the relationship between the image coordinates and the ground points as a ratio of two polynomials. If the original RPCs are directly applied to the bundle block adjustment, there are still discrepancies between the calculated and the true coordinates. To remove these discrepancies, a bias compensation in the bundle block adjustment is required. Grodecki et al. (2003) demonstrated that the bias-compensated RPC block adjustment can provide results with the same accuracy as the physical camera model. The bias compensation RPC block adjustment model defined in object space is nonlinear and also irrelevant to the image geometry. Thus the adjustment model defined in image space is more effective, which was applied in our test scenario. In order to reduce the influence of systematic errors, a natural polynomial model in image space is applied. Discrepancies between measured and calculated coordinates, Δp andΔr, can be represented as:

$$\Delta p = a_0 + a_S * sample + a_L * line + a_{SL} * sample * line + a_{S2} * sample^2 + a_{L2} * line^2 + ... \quad (11)$$

$$\Delta r = b_0 + b_S * sample + b_L * line + b_{SL} * sample * line + b_{S2} * sample^2 + b_{L2} * line^2 + ... \quad (12)$$

where *sample* and *line* are the sample and line coordinates. The parameters a_0, a_L, a_S,…, and b_0, b_L, b_S, …, are the affine coefficients for image coordinates, line and sample are the image coordinates related to a ground control point or tie point. The parameter a_0 and parameter b_0 are offsets in the line and sample direction caused by ephemeris errors, satellite pitch attitude errors and others. It turns out that a_L and b_L can absorb the effects caused by the gyro drift during image scanning, and the parameter a_S and b_S can reduce errors such as radial ephemeris error and interior orientation errors. The rest elements will remove small effects caused by other systematic errors. If the images are not longer than 50 km, the adjustment model can simply use a_0 and b_0. This paper proposes the affine model as the adjustment model for each pair of images, defined as follows:

$$\Delta p = a_0 + a_S * sample + a_L * line \tag{13}$$

$$\Delta r = b_0 + b_S * sample + b_L * line \tag{14}$$

In our case, the full affine correction model, the number and location of GCPs is important which should at least provided by 4 to 6 GCPs. Thus, for each image point i on image j related to ground control point or tie point k, the RPC bundle block adjustment can be described as:

$$line_i^{(j)} = p^{(j)}(\varphi_k, \lambda_k, h_k) + \varepsilon_{Li} + \Delta p^{(j)} \tag{15}$$

$$sample_i^{(j)} = r^{(j)}(\varphi_k, \lambda_k, h_k) + \varepsilon_{Si} + \Delta r^{(j)} \tag{16}$$

Then the observation equation can be represented following Grodecki et al. (2003):

$$F_{Li} = -line_i^{(j)} + p^{(j)}(\varphi_k, \lambda_k, h_k) + \varepsilon_{Li} + \Delta p^{(j)} = 0 \tag{17}$$

$$F_{Si} = -sample_i^{(j)} + r^{(j)}(\varphi_k, \lambda_k, h_k) + \varepsilon_{Si} + \Delta r^{(j)} = 0 \tag{18}$$

where $line_i^{(j)}$ and $sample_i^{(j)}$ are the measured line and sample coordinates of ith image point on image j, which corresponds to the kth ground control or tie point whose object coordinate is (φ_k,λ_k, h_k).
$p^{(j)}(\varphi_k,\lambda_k, h_k)$ and $r^{(j)}(\varphi_k,\lambda_k, h_k)$ are the denormalized image coordinates calculated according to the RPCs:

$$p(\varphi_k, \lambda_k, h_k) = \frac{Num_L(B,L,H)}{Den_L(B,L,H)} * line\_sacle + line\_off \tag{19}$$

$$r(\varphi_k, \lambda_k, h_k) = \frac{Num_S(B,L,H)}{Den_S(B,L,H)} * sample\_sacle + sample\_off \tag{20}$$

ε_{Li} andε_{Li} are the random unobservable errors. $\Delta p^{(j)}$ and$\Delta r^{(j)}$ are the affine model for adjustment of image j.
For this experimental study the bundle block adjustment was carried out in a MatLab environment and finally delivered the affine transformation parameters.

For the Munich testsite 61 GCPs and 23 check points are used – the adjusted results are shown in table 1. Additionally table 2 demonstrates the maximum errors and RMS errors of the image coordinates re-projected from calculated object coordinates. Finally the object coordinates' accuracy is shown in table 3.

Table 1: Adjustment Parameters of WorldView-2 Stereo Imagery Covering the Munich Testsite.

Adjustment Parameters	Left Image of 1st Stereo	Right Image of 1st Stereo	Left Image of 2nd Stereo	Left Image of 2nd Stereo
a_0	23.8338	3.37671	-13.5213	-29.0938
a_s	-0.000127	0.000008	-0.00011	-0.000003
a_l	0.000007	-0.000008	0.000097	-0.000016
b_0	-1.26536	3.43118	7.67870	11.0992
b_s	0.000024	0.000033	0.000024	0.000045
b_l	0.000010	0.000006	-0.000005	0.000006

Table 2: Reprojection Errors of WorldView-2 Stereo Image Covering the Munich Testsite.

	Left image of 1st Stereo		Right image of 1st Stereo	
	line	sample	line	sample
Max Error [pixel]	0.1310	0.5542	0.1313	0.5545
RMS [pixel]	0.0734	0.3100	0.0734	0.3100
	Left image of 2nd Stero		Right image of 2nd Stereo	
	line	sample	line	sample
Max Error [pixel]	0.2302	0.9659	0.2322	0.9654
RMS [pixel]	0.0840	0.3491	0.0841	0.3491

Table 3: Accuracy of WorldView-2 Stereo Image Covering the Munich Testsite

	Latitude	Longitude	Height
Max Error [m]	0.9027	0.8426	2.7265
RMS [m]	0.3951	0.3155	1.3642

4.2. DSM Generation

Using the exterior orientations of the satellite images epipolar images are generated, as input for SURE. Because the WorldView-2 data has two stereos, Fig. 9a just displays one disparity image as an example. According to these disparity images, the object coordinates for each pixel can be calculated by applying forward intersections. All these computing procedures are experimentally implemented using MatLab – first computing the image coordinates of corresponding pixels on epipolar images, then the image coordinates of the original images, and at last the object coordinates. Finally a DSM of 1m GSD is generated by SURE from the WorldView-2 point cloud (Fig. 9b). Obviously, the point cloud generated from WorldView-2 data describes the city well, and most buildings, streets and vegetation are reconstructed clearly.

Figure 9: (a) Munich WV-2 disparity image.

(b) Munich WV-2 DSM@1m GSD.

A first analysis of the reconstructed WV-2 DSM compared with the LiDAR DEM and the aerial photography DSM comes to the following statements:

(a) Using 20 check points on the ground of the LiDAR DEM and the WV-2 DSM delivers a RMS of 2.00m
(b) Using 20 check points on the roofs of the aerial photography DSM and the WV-2 DSM delivers a RMS of 1.41m
(c) Using 20 check points on the ground of the aerial photography DSM and the WV-2 DSM delivers a RMS of 2,09m

Obviously the dense image matching algorithm can deliver disparities along roof surfaces much better than on ground, because of the image noise. Further analyses will follow.

5. CONCLUSIONS

A new family of *Fourier self-calibration APs* for frame-format airborne camera calibration has been introduced. We pointed out, that photogrammetric self-calibration can be considered – to a very large extent – as a *function approximation* problem in mathematics. Fourier APs have solid mathematical foundations: Laplace Equation and Fourier Theorem. The Fourier APs are orthogonal, rigorous, generic, flexible and effective for calibrating frame-format airborne cameras.

The high performance of Fourier APs was identified in many empirical tests. These tests have shown, that Fourier APs can fully calibrate the image distortion of the current airborne cameras, including the DMC, DMC II, UltracamX, UltracamXp and DigiCAM cameras (not all the results could be illustrated in this article). Optimal accuracy can be achieved by using the Fourier APs of proper degree in the blocks of typical in-situ calibration scenario. In principle, the Fourier APs can be used for calibrating the frame airborne cameras of large-, medium- and small-format CCDs, mounted in single- and multi-head systems. The Fourier APs can be combined with radial distortion parameters for calibrating the image distortion with significant radial tendency.

Dense Image Matching (DIM) has a huge impact on photogrammetry, no matter if airborne, spaceborne, close range or mobile applications. All of a sudden photogrammetry became equivalent to laser scanning, although knowing about the obstacles behind both technologies. The Photogrammetric Week 2011 stated that there is no “either or” but “both technologies are complementing each other” – this statement is still true.

During the development of SURE the ifp learned how to understand the formulation and to overcome the problems of Semi-Global Matching and its implementation – we finally decided to implement a tube-based SGM to guarantee faster and more robust solutions. In the last five years many applications have proven the efficiency and generality of this comprehensive software package – also the most recent one processing WorldView-2 stereo imagery.

Maintaining a successful software package in an university environment is very difficult, especially if many customers in industry are relying on the product and are expecting releases continuously. Therefore we think it was a good decision to outsource SURE as an asset of the Startup nFrames – in this way this software package may help many geospatial professionals to solve their daily problems of DIM and to generate added value.

6. ACKNOWLEDGEMENTS

The author gratefully acknowledges the efficient and fruitful cooperation with all staff members of the Institute for Photogrammetry, University of Stuttgart. Many projects have been carried out and many problems were solved – always in a very cooperative way. For this paper the input of Mathias Rothermel und Konrad Wenzel is acknowledged – also the work of Ke Gong. Furthermore, the author is grateful to DLR Oberpfaffenhofen providing the WV-2 stereo scenes and to the LDBV Munich for offering the Munich reference data.

7. REFERENCES

Ackermann, F. (1981): Block Adjustment with Additional Parameters. Photogrammetria 36 (6), pp. 217-227.

Ackermann, F. (1983): High Precision Digital Image Correlation. Proceed. 39. Photogrammetric Week, Stuttgart.

Brown, D. (1971): Close-range Camera Calibration. Photogrammetric Engineering 37 (8), pp. 855-866.

Brown, D. (1976): The Bundle Method – Progress and Prospects. International Archives of Photogrammetry 21 (Part 3), pp. 1-33.

Clarke, T. & Fryer, J. (1998): The Development of Camera Calibration Methods and Models. Photogrammetric Record 16 (91), pp. 51-66.

Cramer, M. (2009): Digital Camera Calibration. EuroSDR Official Publication No. 55.

Cramer, M. (2010): The DGPF Test on Digital Airborne Camera Evaluation – Overview and Test Design. Photogrammetrie – Fernerkundung – Geoinformation (PFG) 2010 (2), pp. 75-84.

El-Hakim, S. & Faig, W. (1977): Compensation of Systematic Image Errors Using Spherical Harmonics. Proc. American Society of Photogrammetry, Fall Technical Meeting, Little Rock, Arkansas, 18-21 October, pp. 492-499.

Ebner, H. (1976): Self-calibrating Block Adjustment. Bildmessung und Luftbildwesen 44 (4), pp. 128-139.

Foerstner, W. (1986): A Feature-based Correspondence Algorithm for Image Matching. Int. Arch. Photogr., Rem. Sens., Vol. 26-III, Rovaniemi.

Fraser, C. (1997): Digital Camera Self-calibration. ISPRS Journal of Photogrammetry and Remote Sensing 52 (4), pp. 149-159.

Fritsch, D., Khosravani, A., Cefalu, A., Wenzel, K. (2011): Multi-Sensors and Multiray Reconstructions for Digital Preservation. In: Photogrammetric Week' 11, Ed. D. Fritsch, Wichmann, Berlin/Offenbach, pp. 305-323.

Fritsch, D. & Rothermel, M. (2013): Oblique Image Data Processing – Potential, Experiences and Recommendations. In: Photogrammetric Week' 13, Ed. D. Fritsch, Wichmann, Berlin/ Offenbach, pp. 73-88.

Fusiello, A., Trucco, E. & Verri, A. (2000): A Compact Algorithm for Rectification of Stereo Pairs. Machine Vision and Applications 12 (1), pp. 16-22.

Gong, Ke (2015): Dense Image Matching of High Resolution Satellite Stereo Data – A Detailed Case Study. Master's Thesis Univ. Stuttgart (not published).

Grimm, P. (2015): IGI Integrated Geospatial Innovations. This proceedings.

Grodecki, J. & Dial, G. (2003): Block Adjustment of High-Resolution Satellite Images Described by Rational Polynomials. Photogrammetric Engineering & Remote Sensing 69 (1), January 2003, pp. 59-58.

Grün, A. (1978): Progress in photogrammetric point determination by compensation of systematic errors and detection of gross errors. International Archives of Photogrammetry 22 (Part 3), pp. 113-140.

Haala, N. (2014): Dense Image Matching Final Report. EuroSDR Official Publication N°64, pp .115-145, 2014.

Hirschmüller, H. (2005): Accurate and Efficient Stereo Processing by Semi Global Matching and Mutual Information. IEEE Conference for Computer Vision and Pattern Recognition, 2, pp. 807-814. San Diego, CA, USA.

Honkavaara, E. (2004): Calibration in Direct Georeferencing: Theoretical Considerations and Practical Results. Photogrammetric Engineering & Remote Sensing 63 (8), pp. 1207-1208.

Jacobsen, K. (2007): Geometric handling of large size digital airborne frame camera images. International Conference on Optical 3D Measurement Techniques VIII, Zürich, 7-9 July, pp. 164-171.

Jacobsen, K., Cramer, M., Ladstätter, R., Ressl, C., Spreckels, V. (2010): DGPF Project: Evaluation of Digital Photogrammetric Camera Systems – Geometric Performance. Photogrammetrie – Fernerkundung – Geoinformation (PFG) 2010 (2), pp. 85-98.

Kazhdan, M. & Hoppe, H. (2013): Screened Poisson Surface Reconstruction. ACM Trans. Graph. 32, 3, Article 29 (June 2013).

Kilpelä, E. (1981): Compensation of systematic errors of image and model coordinates. Photogrammetria 37 (1), pp. 15-44.

Loop, C. & Zhang, Z. (1999): Computing Rectifying Homographies for Stereo Vision. In: IEEE Computer Society Conference on Computer Vision and Pattern Recognition, Fort Collins, USA, pp. 125-131.

McGlone, J., Mikhail, E., Bethel, J., Mullen, R. (Eds.), 2004, Manual of Photogrammetry, fifth ed. American Society of Photogrammetry and Remote Sensing.

Oliver, F., Lozier, D., Boisvert, R., Clark, C. (Eds.) (2010): NIST Handbook of Mathematical Functions, Cambridge University Press, London.

Pajarola, R. (1998): Large Scale Terrain Visualization using the Restricted Quadtree Triangulation. Proc. IEEE Visualization'98, pp. 19-26, 1998.

Pollefeys, M., Koch, R., Van Gool, L. (1999): A Simple and Efficient Rectification Method for General Motion. In: International Conference on Computer Vision, Kerkyra, pp. 496-501.

Rothermel, M., Wenzel, K., Fritsch, D., Haala, N. (2012): SURE: Photogrammetric Surface Reconstruction from Imagery. Proceedings LC3D Workshop, Berlin, December 2012.

Tang, R., Fritsch, D., Cramer, M., Schneider, W. (2012a): A Flexible Mathematical Method for Camera Calibration in Digital Aerial Photogrammetry. Photogrammetric Engineering & Remote Sensing (PERS) 78, pp. 1069-1077.

Tang, R., Fritsch, D., Cramer, M. (2012b): New Rigorous and Flexible Fourier Self-Calibration Parameters for Airborne Camera Calibration. ISPRS Journal of Photogrammetry and Remote Sensing 71, pp. 76-85.

Tang, R. (2013): Mathematical Methods for Camera Self Calibration in Photogrammetry and Computer Vision. Deutsche Geod. Kommission, Reihe C, Nr. 703, München.

Tsingas, V. (1992): Automatisierung der Punktübertragung in der Aerotriangulation durch mehrfache digitale Bildzuordnung. Deutsche Geod. Kommission, Reihe C, Nr. 392, München.

Waechter, M., Moehrle, N., Goesele, M. (2014): Let There Be Color! Large-Scale Texturing of 3D Reconstructions. Proc. ECCV, pp. 836-850, 2014.

Wenzel, K., Rothermel, M., Haala, N., Fritsch, D. (2013): SURE – The ifp Software for Dense Image Matching. Photogrammetric Week ’13, Ed. D. Fritsch, Wichmann, Berlin/Offenbach, pp. 59-70.